富山大学水素同位体機能研究センター研究報告12：59－69，1992.

論　文

無電解Pdめっきによる ZrおよびZr_3Al_2ゲッターの表面改質

芦田　完・渡辺　国昭・諸住正太郎

松田　健二*・多々　静夫*

富山大学水素同位体機能研究センター
富山大学工学部物質工学科*
〒930 富山市五福3190

Surface Modification of Zr and Zr_3Al_2 with Electroless Pd Plating

Kan ASHIDA*1, Kuniaki WATANABE*1, Shotaro MOROZUMI*1

Kenji MATSUDA*2 and Sizuo TADA*2

*1 Hydrogen Isotope Research Center (HRC),
*2 Material Science and Engineering, Faculty of Engineering,
Toyama University, Gofuku 3190, Toyama 930, JAPAN
(Received July 31, 1992; accepted November 9, 1992)

Abstract

Hydrogen storage materials lose their effectiveness in the presence of small amounts of impurity gases in hydrogen owing to the formation of oxide and/or carbide layers on the surface of materials. To avoid this impairment, applicability of Pd coating as protective layer was examined. Zr and Zr_3Al_2 were selected as model substrates and coated with Pd with electroless plating method. The characteristics of the Pd coating were examined with scanning electron microscopy (SEM), electron probe microanalysis (EPMA), x-ray photoelectron spectroscopy (XPS) and thermal desorption spectroscopy (TDS). SEM observations showed that dense and relatively smooth Pd-overlayers could be prepared with this method in combination with vacuum annealing. EPMA and XPS revealed that mutual diffusion of the relevant elements took place above 600℃. As a consequence, the elements of the substrates appeared on the surface. Zr, however, was present as

ZrC, whereas Pd was kept in its pure metallic state. TDS showed that Zr played no important role in absorption and desorption of deuterium and only the Pd-overlayer took part in the ab/desorption processes, indicating that the Pd layer acts as permeation window for hydrogen and can protect the inner substrate from impurity gases.

1. Introduction

Controlled D-T thermonuclear fusion reactors requires safe and reliable fuel processing systems consisting of storage, supply, recovery, separation and purification units. Some metals and alloys forming stable hydrides have potential for these fuel processings. To develop such materials applicable to large scale tritium systems, their physicochemical properties have been investigated from experimental[1~3] as well as theoretical[4~6] view points. These investigations strongly suggest that Zr-based alloys has high potential for the fuel processing systems[7~11].

They show sufficiently low equilibrium pressure at room temperature, a moderate temperature around 500℃ to release hydrogen isotope gases upto 1 atmospheric pressure and considerably high absorption rate for hydrogen isotopes even at low temperatures. In addition, they are not inflammable against air exposure. They, however, lose their activities in the presence of H_2O, CO_2, CO and hydrocarbons, owing to the formation of stable oxide and/or carbide surface layers[12~16].

To avoid this impairment, we have studied effects of surface coatings. As a first step, a Zr plate and Zr_3Al_2 granules were plated with Pd-layers with electroless coating method[17]. This paper describes some findings on the Pd-overlayers observed with scanning electron microscopy (SEM), electron probe micro analysis (EPMA) and x-ray photoelectron spectroscopy (XPS). Furthermore, results of the thermal desorption measurements of deuterium from Pd plated Zr_3Al_2 sample are reported, being focused on the effect of the Pd-overlayers on hydrogen absorption and desorption.

2. Experimental

2. 1. Sample preparation and surface observation

Zr plate (purchased from Material Research Co., 20×20×0.5㎜) and Zr_3Al_2 alloy granules (purchased from Japan Metals & Chemicals Co., ca. 50 mesh) were used as model substrates to prepare surface protective layers. They were plated with Pd with electroless plating method.

The electroless Pd plating was carried out with use of a solution of ethylenediamine ($H_2NCH_2CH_2NH_2$; 0.08 mol/ℓ), palladium (Ⅱ) chloride ($PdCl_2$; 0.01 mol/ℓ) and

thiodiglycolic acid ($S(CH_2COOH)_2$; 10 mg/ℓ) . Before use, 10−20 mℓ of sodium phosphinate solution ($NaPH_2O_2$; 0.04 mol/25 mℓ) was added to 300 mℓ of this solution. Subsequently, the samples were dipped into the solution without stirring, where the temperature was controlled from 40 to 50℃ under argon gas bubbling. The flow rate of argon gas was 100 mℓ/min. After a given plating time, samples were picked up and rinsed twice with distilled water, and then dried at 50℃ in the air. Hereafter, the plated samples are denoted as Pd/Zr for Zr and Pd/Zr_3Al_2 for Zr_3Al_2.

Pd/Zr_3Al_2 was observed with a scanning electron microscope (SEM ; TOPCON, ECP−1) and an electron probe microanalyzer (EPMA ; EDAX 9100) . The Pd/Zr was analyzed with an x-ray photoelectron spectroscope (XPS ; PHI 15−255) . The Mg-K_α radiation was used as probe for XPS. Details of XPS measurements have been described elsewhere[18].

2. 2. Thermal desorption of deuterium

Effects of the Pd-overlayers on the absorption and desorption kinetics were observed with thermal desorption spectroscopy, by using Pd/Zr_3Al_2 as a sample. About 200mg of the sample was loaded to a sample tube made of quartz. The sample tube was set to an oil-free high vacuum apparatus made of stainless steel which was equipped with a quadrupole mass spectrometer (QMS ; ULVAC MSQ-150A) to measure thermal desoption spectra of deuterium. The sample was first activated by vacuum heating above 800℃ for 30 min. Subsequently, it was cooled to 20℃ and exposed to a deuterium gas flow at a given pressure and time to absorb deuterium, and then the system was evacuated to 1×10^{-5} Pa or below at room temperature. Next, the sample was heated to 900℃ with a given linear temperature ramp to desorb the absorbed deuterium. The kinetics of the desorption was analyzed through the observed mass analyzed thermal desorption spectra (TDS) .

3. Results and discussion

3. 1. Surface observation with SEM and EPMA

Figure 1−(a) shows an example of the scanning electron micrograph of the Pd-overlayer on Zr_3Al_2 grown for 10 min. This figure indicates that Pd was deposited in spherical shape of about 1 μm in diameter, although a part of them aggregated each other. Figure 1−(b) shows another part of this sample surface. A large number of smaller particles than those seen in figure 1−(a) appeared, suggesting that the nucleation of Pd is sensitive to heterogeneity of the surface which depends on the defect

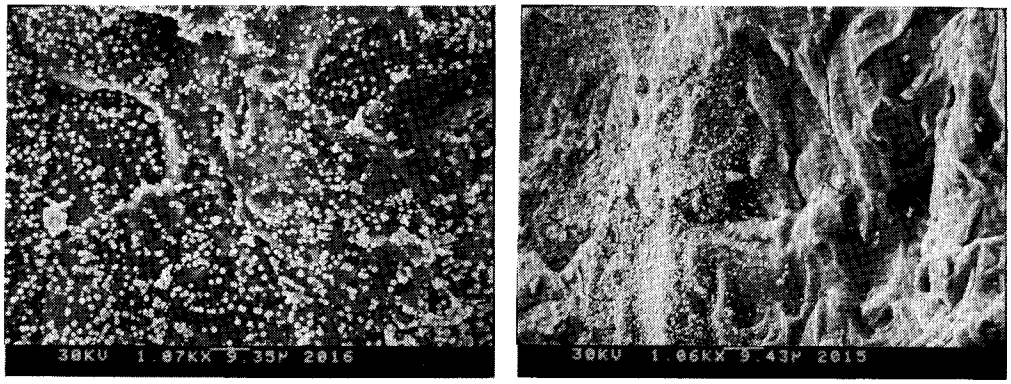

(a) (b)

Fig. 1. Scanning electron micrographs of the Pd/Zr_3Al_2 preparad in 10 min : Pd deposits began to be formed on the substrate.

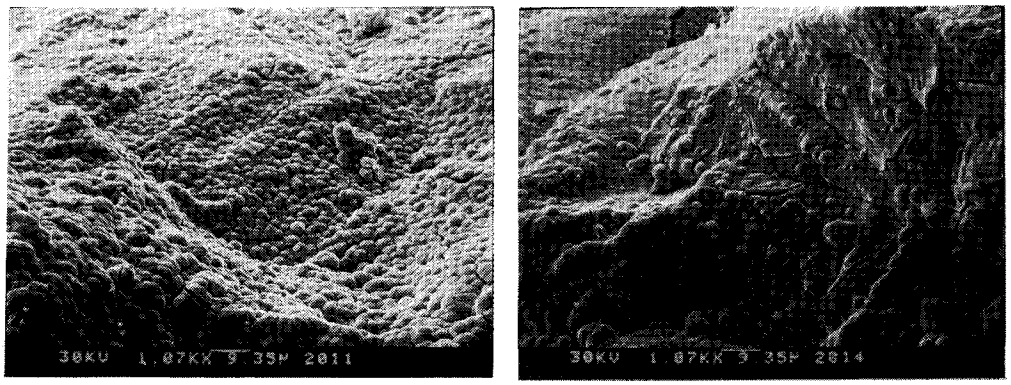

(a) (b)

Fig. 2. Scanning electron micrographs of the Pd/Zr_3Al_2 prepared in 60 min : the whole surface was covered with Pd.

structures and/or crystal faces of a given sample.

Figure 2−(a) and (b) show scanning electron micrographs of the Pd-overlayers on Zr_3Al_2 grown in 60 min. In this case, the whole surface was covered with Pd, although the morphology differed from part to part. The average thickness of the overlayer was estimated as about 2.5 μm from peeled section of the overlayer. This value is valid for both the parts shown in figure 2−(a) and (b). Namely, the average growth rate was estimated about 2.5 μm/hr.

Figure 3−(a) is a scanning electron micrograph of the annealed Pd/Zr_3Al_2 (plated for 60 min) in vacuum at 900℃ for 30 min. This shows that the morphology of the Pd-overlayer was altered by sintering. A similar change in the morphology was observed for other samples. Figure 3−(b) shows mechanically ruptured (left side) and

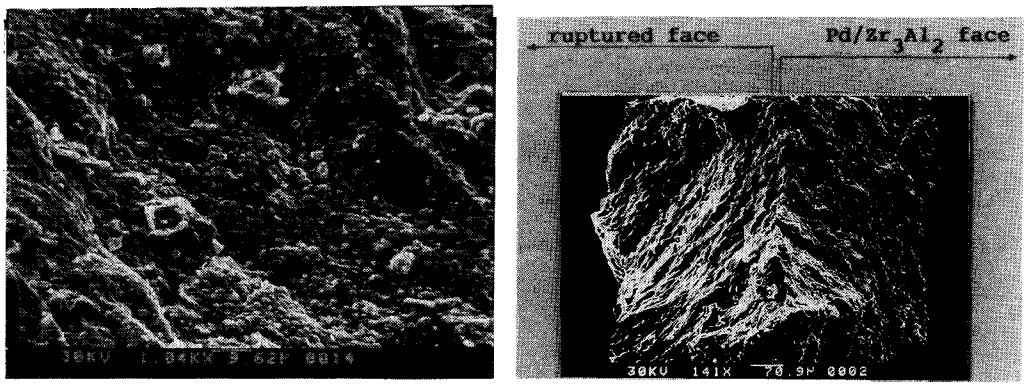

(a) : annealed at 900℃ for 30 min in vacuum.

(b) : mechanically ruptured (left) and sintered (right) face.

Fig. 3. Scanning electron micrographs of the Pd/Zr_3Al_2

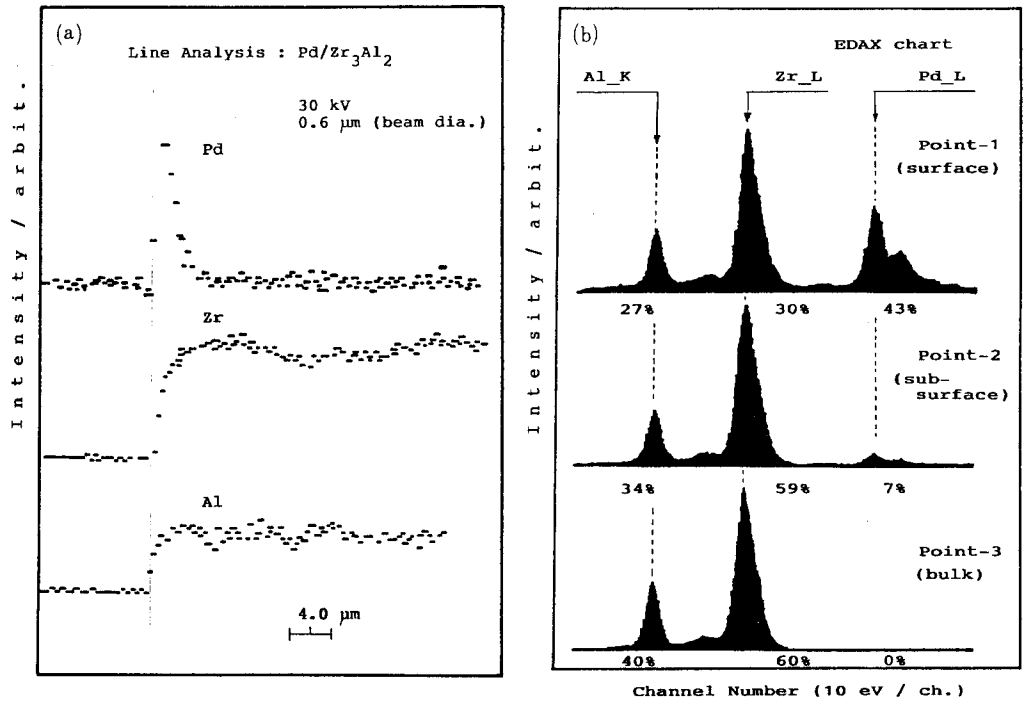

Fig. 4. EPMA analysis of the ruptured face of annealed Pd/Zr_3Al_2 along a line from the surface to the bulk.
(a) : line, and (b) : point analysis mode

sintered (right side) faces of the annealed Pd/Zr_3Al_2, which are divided by the center ridge in the micrograph. Line analysis with EPMA was carried out normal to the fractured surface with scanning from the surface to the bulk direction. Namely, the beam was scanned from an off-sample position to the bulk via the Pd-overlayer zone. Figure

4−(a) shows an example. Three horizontal lines are ground levels of Pd, Zr and Al signals at the off-sample position. The Pd signal jumped up at the surface. It increased with increasing depth and showed a maximum at 2.5 μm from the surface. This value is in good agreement with the thickness of the Pd-overlayer evaluated above. Subsequently, it decreased to the ground level at about 6 μm. On the other hand, the signal intensities of Zr and Al showed reverse movement to that of Pd : they increased from the ground levels at the surface to the steady in the bulk beyond 6 μm depth from the surface.

Figure 4−(b) shows the results of point analyses with EPMA. Point−1, −2 and −3 correspond to different depths from the surface of 1, 3 and 10 μm, respectively. Zr and Al were observed at Point−1, where the atomic ratio of Al to Zr was about unity and that of Pd to Zr about 3/4, as indicated in the figure. Those ratios decreased with depth as about 1/2 for Al to Zr and 7/60 for Pd to Zr, respectively. Eventually, Pd disappeared at the depth of 10 μm and the ratio of Al to Zr became equal to the stoichiometric value of Zr_3Al_2. This means that diffusion of three elements took place at 900℃ and formed a rather thick diffusion layer. In addition, it is seen that the migration of Zr toward the surface was more favored than Al.

3. 2. Surface observation with XPS

Figure 5 shows examples of XPS spectra for Pd/Zr annealed at 100, 500 and 900 ℃ for 10 min in vacuum. Low temperature annealing below 500℃ gave only Pd signals with small impurity peaks of C, O and P. High temperature annealing at 900 ℃ caused the Zr3d peak to appear in the spectrum. With respect to the surface impurities, carbon and oxygen are commonly observed for variety of materials. This is due to adsorbed CO_2,CO and

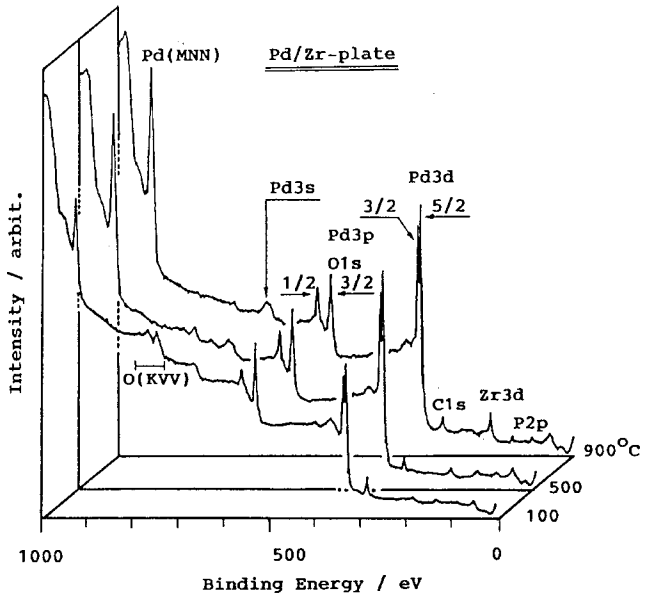

Fig. 5. XPS spectra of Pd/Zr sample annealed at 100, 500, and 900℃

hydrocarbons as well as H_2O which are present in residual gas in vacuum systems and/or in the atmosphere. In this case, it appears also due to the solution used for the electroless Pd plating. Phosphorus apparently arose from the reducing agent used.

Changes in the surface atomic composition with annealing temperature are plotted in figure 6. At the low temperature region below 500℃, the atomic fraction of Pd increased and that of C decreased with temperature. Phosphorus was kept at a constant level about 20 at. %. Namely, the increase in the atomic fraction of Pd with temerature was compensated with the decrease of C. It appears due to desorption of carbon from the surface to gas phase and/or migration of it into the bulk. At the high temperature region above 500℃, Zr appeared and increased its atomic fraction. On the other hand, Pd increased with temperature till 700℃ and then decreased. Carbon showed the reverse movement to that of Pd. The decrease of Pd above 700℃ is a consequence of the increase of Zr and C. At this temperature region, the P fraction showed a slight decrease with temperature but remained at a level of about 10 at. %. The change of the atomic fraction of P with annealing is consistent with literature[19].

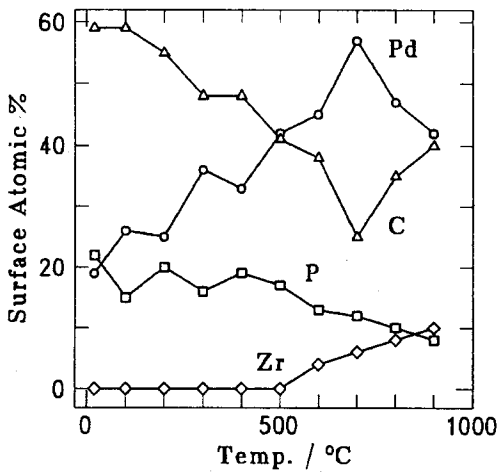

Fig. 6. Changes in the binding energies of Pd/Zr sample with annealing temperature.

Figure 7 shows changes in the binding energies of $Pd3d_{5/2}$, P2p, Cls and $Zr3d_{5/2}$ with annealing temperature, respectively. Figure 7−(a) shows that the Pd-overlayer was kept in pure metallic state throughout the measurements. Figure 7−(b) indicates that P was in both pure and oxide (PO_4) states on the sample surface. The ratio of the former to the latter was roughly 1 : 1 in the low temperature region below 500℃ and the latter

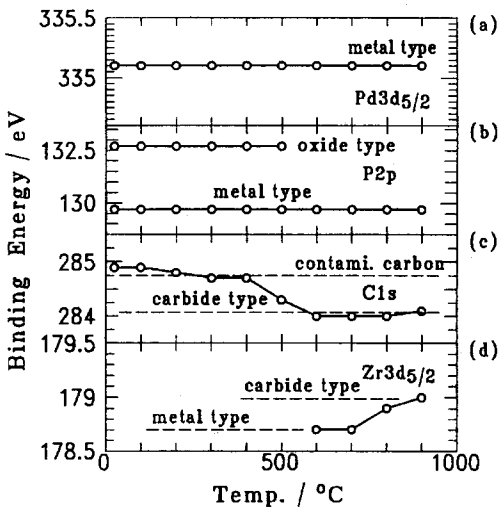

Fig. 7. Changes in the binding energies of (a): $Pd3d_{5/2}$, (b): P2p, (c): Cls, and (d): $Zr3d_{5/2}$ with annealing temperature.

disappeared at 600℃. The binding energy of Cls gradually decreased from 284.9 to 284.0 eV and was kept constant at this value till 900℃. The former is assigned to contaminant carbon and the latter to carbide. Namely, the contaminant carbon initially present on the surface changed to carbide type. This is consistent to the changes in Zr states. Namely, the binding energy of Zr slightly increased from 178.6 to 179.0 eV with temperature, indicating that Zr changed from metallic to carbide above 700℃[20]. This suggests that ZrC accumulated on the surface of Pd/Zr through a reaction of carbonaceous impurity present on the surface with Zr diffused from the substrate. As a consequence, the Pd-overlayer appears to have been covered with ZrC. It is also plausible that ZrC precipitates grew in the Pd matrix. As a result, the surface atomic fraction of Pd decreased with increasing temperature in both cases.

3. 3. Thermal desorption of deuterium

Figure 8 shows TDSs of deuterium for Pd/Zr_3Al_2. Each of these spectra consisted of a single desorption peak and the peak shifted toward lower temperature side with increasing amount of absorption. Similar peak shift has been observed for Zr_3Al_2, where the rate determining step for the desorption is found to be the second order association reaction of deuterium atoms on the sample surface[1]. On the analogy of this fact, we analyzed the present spectra by assuming the second order surface reaction : namely, the desorption rate is described as

$$v_{des} = k_d \sigma^2 \qquad (1)$$

$$k_d = \nu_d \exp(-E_d/RT) \qquad (2)$$

where k_d is the desorption rate constant, ν_d the frequency factor, σ the amount of absorption, and E_d the activation energy for desorption. Differentiating Eq. (1) with T by taking account of $T = T_0 + \beta t$ and $[d(v_d)/dT] = 0$ at the peak temperature, T_P, one obtain

$$\log(T_P^2 \sigma_P/\beta) = (E_d/2.3R)T_P^{-1} + \log(E_d/2R\nu_d) \qquad (3)$$

where β is the linear temperature ramp, σ_P the amount of absorption at peak

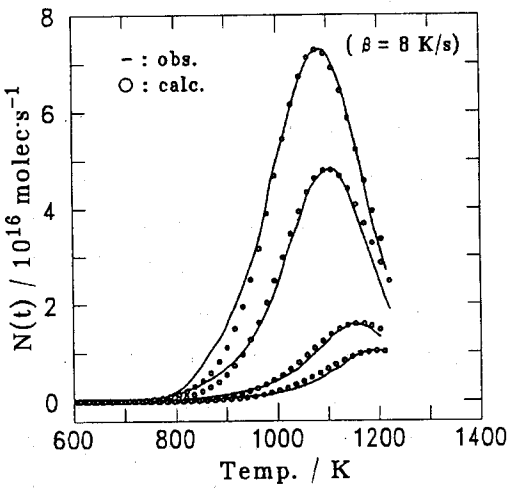

Fig. 8. TDS of deuterium from Pd/Zr_3Al_2 with calculated ones.

temperature. Equation (3) indicates that the plots of $\log(T_P^2 \sigma_P/\beta)$ against $(1/T_P)$ should give a straight line if the desorption process obeys the second order kinetics. Figure 9 shows the plots for Pd $/Zr_3Al_2$. A straight line could be drawn, indicating that the assumption is valid. The activation energy for desorption was determined as 134.4kJ/mol (D_2) for Pd/Zr_3Al_2 from the slope of this line. The pre-exponential factor of desorption for Pd/Zr_3Al_2, ν_d, was evaluated from the intersection of the straight line with vertical axis as 1.3×10^{-13} [molecules^{-1} s^{-1}] . The open circles in figure 8 are examples of the calculated desorption spectra with use a set of evaluated ν_d and E_d, indicating that the desorption process obeys the second order kinetics and the desorption parameters are valid as well. The activation energy described above is greater than that for bare Zr_3Al_2 (106.7 kJ/mol(D_2)). It should be noted, however, the pre-exponential factor evaluated above has not much physical significance, being contrary to the activation energy. This is because the number of active sites on the sample surface was unknown in this study : for example, it will change with sample amount, specific surface area and so on.

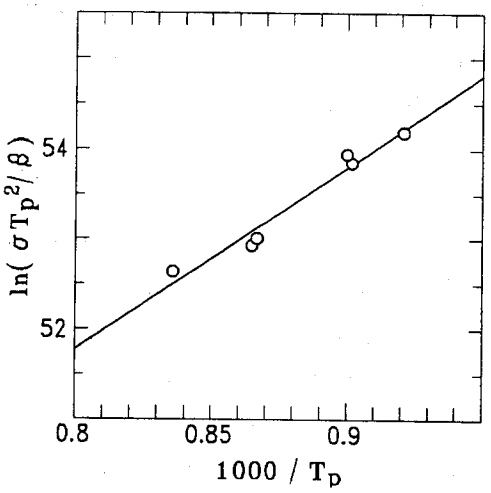

Fig. 9 . Plots of $\ln(T_P^2 \sigma_P/\beta)$ against $(1/T_P)$ for the desorption of D_2 from Pd/Zr_3Al_2.

The desorption kinetics and mechanism for Pd/Zr_3Al_2 are the same as those for Zr_3Al_2 [1]. On the other hand, an effect of Pd plating over Zr_3Al_2 on the desorption of deuterium was apparent in the activation energy. It should be mentioned here that Pd was in the metallic state, whereas Zr was in the carbide state, as seen in figure 7. The activation energy for deuterium desorption described above should compared to Pd. It is reported for polycrystalline Pd that hydrogen desorption obeys the second order kinetics and the activation energy is in a range from 92 to 147 kJ/mol(H_2) [21], depending on preparation conditions. The present value lies in this range.

The absorbed amount of deuterium in the Pd/Zr_3Al_2 sample is calculated by integrating the desorption spectra for deuterium (figure 8) . The maximum uptake of deuterium was [D] / [Pd/Zr_3Al_2] =0.02 in this study. If all of the deuterium was in the Pd-overlayer, its concentration would amount more than [D] / [Pd] =1000. Apparently, this is not plausible : for even Pd-deuteride, it is unity. Consequently, ab-

sorbed deuterium should migrate into Zr_3Al_2 phase. This means that the Pd-overlayer acts as permeation window of hydrogen isotopes, which can protect the inner material from impurity gases.

Conclusions

To avoid the formation of oxide and/or carbide surface layers on Zr-alloy surfaces with O_2, H_2O, CO and so on, the applicability of Pd-overlayer prepared with electroless plating was examined by using Zr and Zr_3Al_2 as model systems. The nucleation of Pd is sensitive to heterogeneity of the surface. The average thickness and growth rate of the Pd-overlayer was estimated to 2.5 μm and 2.5 μm/hr, respectively. Its morphology was altered by sintering. In addition, mutual diffusion between plated Pd and substrate elements, Zr and Al, took place above 600℃ by annealing. However, coated Pd kept pure metallic state at the annealing temperature range from room temperature to 900℃, whereas Zr changed from metallic to carbide states above 700 ℃ by the interactions with surface carbon impurities.

Thermal desorption measurements of D_2 revealed that the desorption obeyed the second order kinetics with respect to the amount of deuterium absorption. The effect of Pd-overlayer to the desorption of deuterium was found in the activation energy. As a consequence, the activation energy increased from 106.7 to 134.4 kJ/mol(D_2) by Pd coating. The latter is in the range reported for polycrystalline Pd. On account of the fact that ZrC grown on the surface appears not to take part in the ad/absorption and desorption of hydrogen, the change in the activation energy should be attributed to the presence of Pd-overlayer. Namely, Pd-overlayer acts as permeation window of hydrogen isotopes, which can protect the inner material from impurity gases such as O_2, H_2O, CO and hydrocarbons.

References

1) M.Watanabe, C.Takeda, S.Tada, H.Anada, S.Ikeno, K.Ashida and K.Watanabe, Fusion Technol., **21** (1992) 763.

2) K.Watanabe, M.Matsuyama, K.Ashida and H.Miyake, J.Vac. Sci. Technol., **A7** (1989) 2725.

3) K.Ichimura, M.Matsuyama and K.Watanabe, ibid., **A5** (1987) 220.

4) P.C.P.Bouten and R.Miedama, J.Less-Common Met., **71** (1980) 147.

5) C.D.Gelatt, H.Ehrenreich and J.A.Weiss, Phys. Rev., **B17** (1979) 1940.

6) F.M.Mueller, A.J.Freemen, J.O.Dimmock and A.M.Furdyna, ibid., **B1** (1976) 4617.

7) T.Yamamoto, T.Yoneoka, S.Kokubo and M.Yamawaki, Fusion Eng. and Design, **7** (1989) 363.

8) K.Watanabe, K.Tanaka, M.Matsuyama and K.Hasegawa, ibid., **18** (1991) 27.

9) R. -D. Penzhorn, M.Devillers and M.Sirch, J. Nucl. Mater., **170** (1990) 217.

10) S.Konishi, T.Nagasaki, N.Yokokawa and Y.Naruse, Fusion Eng. and Design, **19** (1989) 355.

11) K.Watanabe, K.Ichimura, K.Ashida, M.Matsuyama and T.Takeuchi, Fusion Technol., **14** (1988) 729.

12) R. -D. Penzhorn, M.Devillers and M.Sirch, J. Nucl. Mater., **179−181** (1991) 863.

13) K.Ichimura, K.Ashida and K.Watanabe, J. Vac. Sci, Technol., **A3** (1985) 863.

14) M.E.Malinowski, ibid., **A3** (1985) 483.

15) J.L.Cecchi, P.H.LaMache, H.F.Dylla and R.J.Knize, ibid., **A3** (1985) 487.

16) C.Boffito, B.Ferrario and D.Martelli, ibid., **A1** (1983) 1279.

17) "Handbook of Precious Metals", ed. by E.M.Saviskii, Hemisphere Publishing Co., 1984.

18) K.Ichimura, N.Inoue, K.Ashida, K.Watanabe and T.Takeuchi, J. Nucl. Mater., **128/129** (1984) 876.

19) S.Mizumoto, H.Nawafune, E.Uchida and M.Haga, Hyoumen Gijyutu, **40** (1989) 477. (in Japanese)

20) "Handbook of x-ray photoelectron spectroscopy", ed. by G.E.Muilenberg, Perkin-Elmer, 1978.

21) A.W.Aldag and L.D.Schmidt, J. Catal., **22** (1971) 260.